ZEUS-pub-06-007-draft

Submitted to the
XXXIII International Conference on High Energy Physics
July 26 - August 2, 2006, Moscow, Russia

Abstract: -

Session: QCD hard interactions
Heavy Quark physics

Measurement of open beauty production at HERA in the $D^*\mu$ final state

ZEUS Collaboration

21 July 2006

Abstract

The production of beauty quarks with a $D^{*\pm}$ and a muon in the final state has been measured with the ZEUS detector at HERA using an integrated luminosity of 114 pb^{-1}. Low transverse-momentum thresholds for the muon and D^* meson allow a measurement of beauty production closer to the production threshold than previous measurements. The beauty signal was extracted using the charge correlations and angular distributions of the muon with respect to the D^* meson. Cross sections for photoproduction and deep inelastic scattering are somewhat higher than, but compatible with, next-to-leading-order QCD predictions, and compatible with other measurements.

1 Introduction

The production of beauty quarks in ep collisions at HERA is a stringent test for perturbative Quantum Chromodynamics (QCD) since the large b-quark mass ($m_b \sim 5\,\mathrm{GeV}$) provides a hard scale that should ensure reliable predictions. For b-quark transverse momenta comparable to the b-quark mass, next-to-leading-order (NLO) QCD calculations in which the b quarks are generated dynamically are expected to provide accurate predictions [1, 2].

The beauty-production cross section has been measured in $p\bar{p}$ collisions at the S$p\bar{p}$S [3] and Tevatron colliders [4], in $\gamma\gamma$ interactions at LEP [5], and in fixed-target πN [6] and pN [7] experiments. While most results, including recent results from the Tevatron, are in agreement with QCD predictions, some, in particular those from LEP, show large discrepancies.

This paper reports a measurement of beauty production via the reaction $ep \rightarrow eb\bar{b}X \rightarrow eD^*\mu X'$ using the ZEUS detector at HERA. This reaction offers the advantage of providing a data sample enriched in b quarks and with strongly suppressed backgrounds from other processes, which allows low-p_T threshold cuts to be applied. This analysis therefore complements HERA measurements based on leptons and/or jets with high transverse momentum [8–11]. A similar measurement has been performed by the H1 collaboration [12].

Of particular interest are events in which the muon and D^* originate from the same parent B meson (Fig. 1a), e.g. $B^0 \rightarrow D^{*-}\mu^+\nu_\mu$. These yield unlike-sign D^*-muon pairs produced in the same detector hemisphere and with invariant mass below the B-meson mass. Another important contribution arises from charm-pair production, where one charm quark fragments into a D^* and the other decays into a muon (Fig. 1b). This again yields unlike-sign D^*-muon pairs, but with the D^* and the muon produced predominantly in opposite hemispheres. In addition, beauty-pair production in which the D^* and muon originate from different beauty quarks can yield both like- and unlike-sign D^*-muon combinations, depending on whether the muon is from the decay of the primary beauty quark (Fig. 1c), or from a secondary charm quark (Fig. 1d), and whether B^0-$\bar{B}^0$ mixing has occured.

Background contributions to both like- and unlike-sign combinations include events with either fake D^* mesons, originating from combinatorial background, or fake muons. In this analysis, the signal is extracted from the unlike-sign sample, while the like-sign sample is used as a cross check.

Cross sections are extracted separately for the photoproduction (γp, photon virtuality $Q^2 \lesssim 1$ GeV^2), and deep inelastic scattering (DIS, $Q^2 \gtrsim 1$ GeV^2) regimes, as well as for the entire range in Q^2, which includes the kinematic region in which these two event classes cannot easily be distinguished.

2 Experimental set-up

The data sample used in this analysis corresponds to an integrated luminosity $\mathcal{L} = 114.1 \pm 2.3\ \mathrm{pb}^{-1}$, collected by the ZEUS detector in the years 1996-2000. During the 1996-97 data taking, HERA provided collisions between an electron[1] beam of $E_e = 27.5\,\mathrm{GeV}$ and a proton beam of $E_p = 820\,\mathrm{GeV}$, corresponding to a centre-of-mass energy $\sqrt{s} = 300\,\mathrm{GeV}$ ($\mathcal{L}_{300} = 38.0 \pm 0.6\ \mathrm{pb}^{-1}$). In the years 1998-2000, the proton-beam energy was $E_p = 920\,\mathrm{GeV}$, corresponding to $\sqrt{s} = 318\,\mathrm{GeV}$ ($\mathcal{L}_{318} = 76.1 \pm 1.7\ \mathrm{pb}^{-1}$).

A detailed description of the ZEUS detector can be found elsewhere [13]. A brief outline of the components that are most relevant for this analysis is given below.

Charged particles are tracked in the central tracking detector (CTD) [14], which operates in a magnetic field of 1.43 T provided by a thin superconducting coil. The CTD consists of 72 cylindrical drift chamber layers, organized in 9 superlayers covering the polar-angle[2] region $15^\circ < \theta < 164^\circ$. The transverse-momentum resolution for full-length tracks is $\sigma(p_T)/p_T = 0.0058 p_T \oplus 0.0065 \oplus 0.0014/p_T$, with p_T in GeV.

The high-resolution uranium-scintillator calorimeter (CAL) [15] consists of three parts: the forward (FCAL), the barrel (BCAL) and the rear (RCAL) calorimeters. The smallest subdivision of the calorimeter is called a cell. The CAL energy resolutions, as measured under test-beam conditions, are $\sigma(E)/E = 0.18/\sqrt{E}$ for electrons and $\sigma(E)/E = 0.35/\sqrt{E}$ for hadrons, with E in GeV.

The position of electrons scattered at small angles to the electron beam direction was measured using the small-angle rear tracking detector (SRTD) [16, 17]. The SRTD is attached to the front face of the RCAL and consists of two planes of scintillator strips, arranged orthogonally. The strips are 1 cm wide and 0.5 cm thick.

The muon system consists of rear, barrel (R/BMUON) [18] and forward (FMUON) [13] tracking detectors. The B/RMUON consists of limited-streamer (LS) tube chambers placed behind the BCAL (RCAL), inside and outside a magnetized iron yoke surrounding the CAL. These chambers cover polar angles from 34^o to 135^o and from 135^o to 171^o, respectively.

---

[1] Electrons and positrons are not distinguished in this paper and are both referred to as electrons.

[2] The ZEUS coordinate system is a right-handed Cartesian system, with the Z axis pointing in the proton beam direction, referred to as the "forward direction", and the X axis pointing left towards the centre of HERA. The coordinate origin is at the nominal interaction point. The pseudorapidity is defined as $\eta = -\ln\left(\tan\frac{\theta}{2}\right)$, where the polar angle, θ, is measured with respect to the proton beam direction.

The luminosity was measured using the bremsstrahlung process $ep \to ep\gamma$. The resulting small-angle energetic photons were measured by the luminosity monitor [19], a lead-scintillator calorimeter placed in the HERA tunnel at $Z = -107$ m.

3 Data Selection

The data were selected online via a three-level trigger system through a combination of three different trigger chains.

- A muon reaching the inner B/RMUON chambers and matched to a minimum ionizing energy deposit in the CAL or any muon reaching the outer B/RMUON chambers or
- a D^* candidate [20] or
- a scattered-electron candidate in the CAL [11]. In part of the data taking, the cuts on the electron candidate were relaxed if a muon in the inner B/RMUON chambers was detected.

Due to this redundancy, the trigger efficiency for beauty events was high, 94 ± 3 % for the inclusive study, and 98 ± 2 % for the DIS selection.

Muons were reconstructed offline using the following procedure: a track was found in the inner B/RMUON chambers, then a match in position and angle to a CTD track was required. In the bottom region of the detector, where there are no inner chambers, the outer chambers were used instead. If a match was found to both inner and outer chambers, a momentum matching criterion was added.

The angular coverage of the B/RMUON and of the track requirements in the CTD restrict the muon acceptance to the pseudorapidity region

$$-1.75 < \eta^\mu < 1.3 \ . \tag{1}$$

A cut on the muon transverse momentum

$$p_T^\mu > 1.4\,\mathrm{GeV} \tag{2}$$

was applied, reflecting the requirement that the muon reaches the inner muon chambers in the barrel region. In order to have uniform kinematic acceptance, this cut was also applied in the rear region.

D^* candidates were reconstructed in the $D^{*+} \to D^0(\to K^-\pi^+)\pi_s^+$ decay channel (+c.c.) making use of the ΔM ($\equiv M(K\pi\pi_s) - M(K\pi)$) technique described in previous publications (e.g. [20]) with the following cuts:

$$\begin{array}{rl} D^0 \text{ mass} & 1.81 < M(K\pi) < 1.92\,\text{GeV}; \\ D^* - D^0 \text{ mass difference} & 0.1435 < \Delta M < 0.1475\,\text{GeV}; \\ D^* \text{ transverse momentum} & p_T^{D^*} > 1.9\,\text{GeV}; \\ D^* \text{ pseudorapidity} & |\eta^{D^*}| < 1.5; \\ K,\pi \text{ transverse momentum} & p_T^{K,\pi} > 0.5\,\text{GeV}; \\ \text{slow pion} & p_T^{\pi_s} > 0.125\,\text{GeV}. \end{array} \tag{3}$$

To allow the background to the D^* signal to be determined, D^0 candidates with wrong-charge combinations, in which both tracks forming the D^0 candidates have the same charge and the third track has the opposite charge, were also retained.

The hadronic system was reconstructed from the calorimeter information and the reconstructed vertex. A four-momentum $(p_X^i, p_Y^i, p_Z^i, E^i)$ was assigned to each calorimeter cell. Global hadronic variables were reconstructed by summing over these cells. In the case of identified DIS events (see below), the scattered electron candidates were excluded from this sum. The inelasticity y was reconstructed from the Jacquet-Blondel estimator $y_{\text{JB}} = (E - P_Z)/2E_e$ [21], where $E - P_Z = \sum_i (E^i - p_Z^i)$ and the sum runs over all cells. In the case of DIS events, the alternative value $y_e = 1 - \frac{E'_e}{2E_e}(1 - \cos\theta_e)$ as well as the photon virtuality Q^2 were obtained from the energy E'_e and scattering angle θ_e of the final-state electron candidate [11]. A sample of events with one muon and one D^* candidate was selected by requiring:

- ≥ 1 muon in the muon chamber regions defined by Eq. (1) and Eq. (2);
- ≥ 1 D^* candidate in the D^* acceptance region defined by Eq. (3);
- the muon candidate track is not one of the three D^* candidate tracks, eliminating backgrounds from semileptonic D^0 decays;
- the $D^*\mu$ system carries a significant fraction of the total transverse energy of the event, $p_T^{D^*\mu}/E_T > 0.14$, where E_T is the transverse energy measured by the CAL outside a cone of 10° around the proton beam direction to exclude the proton remnant, and $p_T^{D^*\mu}$ is the transverse momentum of the $D^*\mu$ system, reducing combinatorial D^* background;
- a reconstructed vertex compatible with the nominal interaction point, suppressing non-*ep* background.

After this selection, a sample of 232 events remained. The resulting ΔM distributions for the like and unlike $D^*\mu$ charge combinations, before the ΔM cut, are shown in Figs. 2a and 2b.

A subsample of photoproduction events was selected by requiring:

- no scattered-electron candidate found in the CAL;
- $E - P_Z < 34\,\text{GeV}$

retaining 81% of the inclusive sample. After the unfolding of the detector response, these cuts correspond to an effective cut $Q^2 < 1\,\text{GeV}^2$ and $0.05 < y < 0.85$. The lower limit on y arises from the interplay between the b-quark mass and the acceptance in rapidity.

Alternatively, a clean DIS sample was obtained by applying the following additional conditions [11]:

- a reconstructed electron with energy E'_e >10 GeV;
- $Q^2 > 2$ GeV^2;
- inelasticity $y_{\text{JB}} > 0.05$ and $y_e < 0.7$;
- $40 < E - P_Z < 60\,\text{GeV}$;
- the electron hits the rear calorimeter outside a rectangle of $|X| < 13$ cm and $|Y| < 7$ cm.

These cuts correspond to an effective cut $Q^2 > 2\,\text{GeV}^2$ and $0.05 < y < 0.7$. For this sample, which contains less combinatorial background, the D^* cuts were relaxed to

$$\begin{aligned} p_T^{D^*} &> 1.5\,\text{GeV}; \\ p_T^{K,\pi} &> 0.4\,\text{GeV}; \\ p_T^{\pi_s} &> 0.12\,\text{GeV}; \end{aligned} \tag{4}$$

and the cut on $p_T^{D^*\mu}/E_T$ was dropped. All other cuts on the D^* and the muon remained unchanged. A sample of 44 events was obtained. The resulting ΔM distributions for the like and unlike $D^*\mu$ charge combinations are shown in Figs. 2c and 2d.

4 Backgrounds and event simulation

Several contributions to the selected data sample were evaluated:

- the signal from beauty decays;
- the background from fake D^* combinations;
- the $D^*\mu$ background from charm decays;
- the background from fake or non-prompt muons with a real D^* from charm.

The number of background events under the D^* mass peaks (fake D^*) was estimated using the wrong-charge $K\pi$ combinations combining the like- and unlike-sign samples. Wrong-charge combinations were normalised to the data outside the D^* peak in the side-band

$0.15 < \Delta M < 0.17\,\text{GeV}$, separately for the like-sign and unlike-sign $D^*\mu$ sample, as shown in Fig. 2. Dedicated studies [22] performed by selecting data on the D^* side-band showed that this sample correctly reproduces shape and normalisation of the fake-D^* background for the relevant variables used in the analysis.

Monte Carlo (MC) simulations of beauty and charm production were performed using the Pythia [23], Rapgap [24] and Herwig [25] generators. These simulations are based on leading-order matrix elements complemented by parton showers to obtain higher order topologies. Direct photon-gluon-fusion process ($\gamma g \to Q\bar{Q}$, $Q = b, c$), flavour excitation in the resolved photon and proton (e.g. $Qg \to Qg$, $\gamma Q \to Qg$), and hadron-like resolved photon processes ($gg \to Q\bar{Q}$) were included. Gluon splitting into heavy flavours ($g \to Q\bar{Q}$) in events with only light quarks in the hard scattering was not included in the simulations; this contribution is, however, expected to be small [22]. For all generated events, the ZEUS detector response was simulated in detail using a programme based on GEANT 3.21 [26].

Fake muons can be produced by hadron showers leaking from the back of the calorimeter or by charged hadrons traversing the entire calorimeter without interaction. In addition, low-momentum muons can originate from in-flight decays of pions and kaons. It is also possible for tracks reconstructed in the central tracker to be wrongly associated to a signal from a real muon in the muon chambers. A dedicated study [22] based on pions from K^0 decays, protons from Λ decays, and kaons from ϕ and D^* decays, showed that the detector simulation reproduced these backgrounds reasonably well. Most fake muons are associated with fake D^* candidates, and therefore accounted for in the fake-D^* background estimated directly from the data. Fake muons associated with a real D^* are included in the charm and beauty MC samples.

Distributions of variables used in the event selection or relevant for the event kinematics, for the unlike-sign inclusive sample, are compared to the expectations from these simulations in Fig. 3, separately for the beauty- and charm-enriched regions defined in Section 5. Agreement with expectations is obtained, apart from some possible deviations in the $p_T^{D^*\mu}$ and $p_T^{D^*\mu}/E_T$ distributions which are accounted for in the systematic uncertainties (Section 7).

5 Signal extraction

In this section, the signal-extraction procedure is described for the inclusive sample. The γp subsample and the DIS sample were treated in an analogous way.

Figures 4a and 4b show the distribution of the angular difference $\Delta R = \sqrt{\Delta\phi^2 + \Delta\eta^2}$ between the D^* and the muon, where ϕ is the azimuthal angle, and the mass of the $D^*\mu$ system for events passing all selections, including the ΔM cut. The distributions are shown separately for like- and unlike-sign $D^*\mu$ events. The expected signal and background contributions, normalised to the fractions determined later in the analysis, are also indicated. For unlike-sign events, the region $\Delta R > 2$, which mainly corresponds to the back-to-back configuration, is clearly dominated by events from charm. Indications that the simulated distribution might be more sharply peaked than the data turned out to have little influence on the determination of the beauty fraction. In contrast, the region $\Delta R < 2$ is enriched in beauty events, in which the D^* and muon originate mainly from decays of the same parent B hadron. This is illustrated further in the $D^*\mu$ invariant-mass distribution (Figs. 4c and 4d) for events in the beauty-enriched region ($\Delta R < 2$). A peak with an upper edge close to 5 GeV, which can be attributed to the partial reconstruction of the decaying B meson, is clearly visible. A comparison with the like-sign sample shows that the low-mass edge of this peak is dominated by background. An invariant-mass cut of 3 GeV $< M(D^*\mu) <$ 5 GeV was therefore applied to the $\Delta R < 2$ subsample.

The ΔR and $\Delta\phi$ distributions, after this additional cut and after statistical subtraction of the fake-D^* background, are shown in Figs. 5a and 5c, together with two component a fit of the relative contributions from charm and beauty. The fake-muon background with a real D^* from charm, which is treated as part of the charm component, is shown separately. The small fraction of fake muons from beauty was included was included in the beauty component. The fit result for the fraction of beauty events in the final inclusive sample shown in Figs. 5a and 5c, using the shapes predicted by Pythia, is:

- $f_b = 0.307 \pm 0.064$(stat.) for the ΔR and
- $f_b = 0.290 \pm 0.062$(stat.) for the $\Delta\phi$ distribution.

The ΔR result was chosen as the reference, and the $\Delta\phi$ result used as a systematic check. With these fitted fractions, the breakdown into the corresponding number of beauty, charm, and fake-muon candidates in each subsample is given in Table 1. In the unlike-sign part, the beauty and charm contributions are now separated, with only small cross-contaminations. The normalisation of the beauty and charm contributions in Fig. 4 already reflects these fitted fractions. Agreement is seen, also in the like-sign part, which was not included in the fit.

The results from the application of the same procedure to the γp subsample are also shown in Table 1. The analogous results for the DIS sample are shown in Figs. **??**b. and **??**d. The $\Delta\phi$ distribution gives less discrimination in this case, due to the transverse boost from the exchanged virtual photon. Therefore, the $M(D^*\mu)$ distribution was used. The fitted beauty fractions in the DIS sample, using the shapes predicted by Rapgap, are

- $f_b = 0.55 \pm 0.25$(stat.) for the ΔR and
- $f_b = 0.43 \pm 0.30$(stat.) for the $M(D^*\mu)$ distribution.

Again, the ΔR result is chosen as the reference, and the other as a cross check. The breakdown into different event categories is shown in Table 1. The acceptance corrections for the cross sections which will be presented in section 8 were evaluated using PYTHIA for $Q^2 < 1\,\mathrm{GeV}^2$, RAPGAP for $Q^2 > 1\,\mathrm{GeV}^2$, and HERWIG as a systematic check.

6 Theoretical predictions and uncertainties

For direct comparisons with QCD, next-to-leading-order (NLO) predictions were used. Calculations in which b quarks are treated as massless particles [27] are not applicable in this kinematic range, while calculations based on alternative parton-evolution schemes [28] do not yet exist with full NLO implementation. Fixed-order NLO calculations with massive b quarks should yield accurate predictions. Different types of such predictions were evaluated.

The FMNR program [1] evaluates cross sections for next-to-leading-order beauty production in γp collisions in the fixed-order massive approach, for both point-like and hadron-like photon coupling to the heavy quarks. The parton-density functions used were CTEQ5M [29] for the proton and GRV-G-HO [30] for the photon. The renormalisation and factorisation scales μ were chosen to be equal and parametrised by $\mu_0 = \sqrt{p_T^2 + m_b^2}$, where p_T^2 is the average of the squared transverse momentum of the two emerging b quarks and $m_b = 4.75$ GeV. An estimate of the theoretical uncertainty was obtained by simultaneously varying $4.5 < m_b < 5.0$ GeV and $\mu_0/2 < \mu < 2\mu_0$ such that the uncertainty was maximised. Typical uncertainties resulting from this procedure (e.g. for the $b\bar{b}$ total cross section) are +40% and -25%. Variations of the parton densities led to uncertainties which were much smaller than the uncertainties related to mass and scale variations. They were therefore neglected.

Predictions at the level of visible $D^*\mu$ final states are needed in addition to those at parton level. The FMNR program provides a framework to fragment b quarks into B hadrons, and simulate the decay of these hadrons by interfacing them to appropriately chosen decay spectra. However, decays to complex final states, such as a D^* and μ from the same B hadron with cuts on both particles, cannot be easily implemented in this scheme. A straightforward interface of the parton-level events produced by FMNR to MC-like fragmentation and decay chains is also impracticable, since these events have positive and negative weights spanning more than 8 orders of magnitude, making such an approach extremely inefficient.

These difficulties were overcome in a two-step process. In the first step, two ore more FMNR parton-level events with large positive and negative weights and similar topology are combined into events with much smaller weights by averaging the parton momentum vectors [31]. Events are considered to have similar topology if the differences in transverse momentum, rapidity and azimuthal angle of the b quarks are less than user cut values, that reflect the detector resolution. Furthermore, events with small weights were sampled with a probability proportional to their weight. In this way, the weight range was reduced to about two orders of magnitude. It was explicitly checked that this procedure preserves the NLO accuracy for the relevant cross sections at parton level (e.g. b quark p_T and angular distributions).

In the second step, these parton-level events were interfaced to the PYTHIA/JETSET [32] fragmentation and decay chain, making use of the full decay tables and decay kinematics implemented in PYTHIA 6.2. Therefore, non-dominant complex decays, such as $B \rightarrow D^*D$ followed by $D \rightarrow \mu X$, or muons produced through intermediate J/ψ or τ states, were automatically included. The initial-state partons were allowed to have intrinsic k_T (typically $\sim$ 300 MeV) as implemented in PYTHIA. This has a negligible effect on the resulting cross sections ($\sim$ 1%). Parton showering was not included in order to avoid double counting of higher-order contributions[3].

Fragmentation of b quarks close to production threshold is non-trivial. The details of the threshold treatment were found to be much more important than the choice of a particular fragmentation function. The Peterson formula [34] with $\epsilon = 0.0035$ was used. Three approaches were considered:

- independent fragmentation as implemented in PYTHIA [32]. The use of this quite old model was motivated by the fact that FMNR does not provide colour connections on an event-by-event basis;
- fragmentation in the Lund string model [35], again as implemented in PYTHIA. For this purpose, reasonable colour connections were assigned to each event;
- the independent fragmentation scheme provided within the FMNR framework, rescaling the B-hadron momentum to a fraction of the b-quark momentum according to the Peterson formula, which is a somewhat crude approximation at threshold.

The second option was used for all central predictions. The first option was used to obtain the lower systematic error (typically -5%). The third option could not be applied directly, since it does not provide cross-section predictions for correlated final states from the same b quark, as needed here. Instead, it was applied to a cross section in which the final-state correlations originate from different b quarks only, which is more easily calculable in this scheme. The results were used to evaluate a generic upper systematic error of +15% on the fragmentation procedure close to b production threshold. The effect

[3] The MC@NLO approach [33], which does allow the combination of NLO matrix elements with parton showers, is not yet available for ep interactions.

of a variation of the Peterson parameter ϵ in the range 0.0023 to 0.0045 was found to yield uncertainties which were much smaller than the uncertainties due to the different fragmentation procedures. It was therefore neglected.

The branching fractions were corrected to correspond to those obtained from the Particle Data Group [36], as listed in Table 2. Branching fraction uncertainties result in uncertainties on the $D^*\mu$ cross section of typically $\pm12\%$.

In principle, FMNR predictions are only valid for the photoproduction regime. The Weizsäcker-Williams approximation with an effective $Q^2_{\rm max}$ cutoff of 25 GeV^2 ($\sim m_b^2$) [37] was used to include the $\sim$15% DIS contribution to the combined cross section.

Alternatively, the DIS part can be calculated using the NLO predictions from HVQDIS [2]. Only point-like contributions are included in this prediction. The parton density function used was CTEQ5F4 [29]. The renormalisation and factorisation scales μ were chosen to be equal and parametrised by $\mu_0 = \sqrt{Q^2 + m_b^2}$. Mass and scales were varied as for FMNR. A scheme for the calculation of visible cross sections for correlated final states, corresponding to the FMNR$\otimes$PYTHIA interface described above, was not available. Therefore, cross-section comparisons in DIS are limited to the parton level.

7 Systematic uncertainties

The main experimental uncertainties are described below, in order of importance. Numbers in parentheses are quoted for the inclusive selection. Uncertainties for the γp results are also quoted when they differ significantly from the inclusive results. For the DIS sample, the statistics were often too small to derive meaningful systematic errors. The errors from the inclusive sample were used instead.

- **Simulation of $\boldsymbol{p_T^{D^*\mu}}$.** The largest error arises from the observation that the muon and D^* p_T spectra in the b signal region of the data ($\Delta R(D^*\mu) < 2$, $3 < M(D^*\mu) < 5$ GeV) appear to be somewhat softer than predicted by the Monte Carlo simulations (Fig. 3). The differences are concentrated at small values of $p_T^{D^*\mu}/E_T$. Since the corresponding spectra are well reproduced in the charm region with larger statistics, this cannot be attributed to problems with the muon or D^* reconstruction. There are several ways to interpret these differences:

  a) they are statistical fluctuations. This assumption leads to the central result reported;

  b) the signal distribution is significantly softer than predicted by QCD. Due to the rising efficiency as a function of p_T^b, this would change the efficiency calculation for the measurement of the visible cross section. To evaluate this possibility, the MC

$p_T^{D^*\mu}$ (true level) distribution in the signal region was reweighted to be compatible at the 1 σ level with the measured $p_T^{D^*\mu}$ spectrum of the inclusive sample (Fig. 3) (+14%);

c) there is an additional unknown background contribution at low p_T, which occurs only in the beauty-enriched region. There is no indication that this is the case. Nevertheless, to account for this possibility, the $p_T^{D^*\mu}/E_T$ cut was tightened from 0.14 to 0.2, which removes most of the differences (Fig. 3) (-33% for inclusive, -18% for γp selection).

- **Branching fractions**. The beauty-enriched region, which dominates the fit result, is mainly populated by events in which the D^* and μ originate from the same b. The rate of these events depends on different branching fractions from those relevant to the charm-enriched region, in which the D^* and μ originate from different b quarks. A variation of these branching fractions, within the uncertainties quoted in Table 2, therefore affects the shape of the beauty contribution and the fitted beauty fraction ($\pm$8%).
- **Fragmentation and parton showering**. The HERWIG MC uses a different fragmentation model from that of PYTHIA and RAPGAP. It also yields different $b\bar{b}$ correlations from direct/resolved contributions and parton showering. This leads to differences in the acceptance, and in the fitted beauty fraction (+5/-8%).
- **Signal-extraction procedure**. In addition to statistical fluctuations, different ways to fit the data can yield systematic differences due to binning effects and different systematics for different variables, e.g. imperfections in the shape of the MC distributions. To check the error from this effect, the cross sections were evaluated using different procedures: fits to $\Delta R(D^*\mu)$, $\Delta\phi(D^*\mu)$, $M(D^*\mu)$, and simple event counting. In all cases the differences were well within the quoted errors. To avoid double counting of statistical and systematic errors, these were used as cross checks only.
- **Uncertainty on the estimation of the muon chamber efficiency**. Corrections to the MC muon chamber reconstruction efficiency were obtained from independent data samples and varied within their uncertainties ($\pm$5%).
- **Fake muon background**. The background from fake muons has been extensively studied [22] and is further constrained by the like-sign distribution of Fig. 4c, which is dominated by this background. Accordingly it was varied by a factor 1.5 (-4%).
- **Luminosity measurement**. The uncertainty associated with the luminosity measurement for the 1996-00 data taking periods used for this analysis ($\pm$2%).
- **Tracking**. All tracking-based cuts (p_T and mass cuts) were varied by their respective uncertainties. To avoid double counting of statistical uncertainties, the D^*-related

systematics were taken from previous ZEUS DIS ([38]) and γp ([39]) analyses employing similar cuts but with larger event samples The cut on p_T^μ was varied by ± 40 MeV. This yielded a combined error of +6% and -4%.

- **Trigger acceptance**. The error on the trigger acceptance was evaluated by comparing the efficiencies of the different trigger chains in the data with each other and with the MC ($\pm 3\%$).
- **B^0-$\bar{B}^0$ mixing**. The possible systematic effect due to the variation of the mixing rate was found to be negligible.

The total systematic uncertainty was obtained by adding the above contributions in quadrature.

8 Results

To present results from the combined data sets, the measurements from the 1996-97 run have been corrected using the predicted cross section ratio [1] of 1.06, to correspond to the higher center-of-mass energy of 318 GeV. All cross sections are therefore quoted for $\sqrt{s} = 318$ GeV.

8.1 Visible cross sections

The first step is the extraction of visible cross sections for the $D^*\mu$ final state from beauty. The acceptance for the $D^* \to D^0\pi_s \to (K\pi)\pi_s$ decay chain was unfolded using a branching fraction of 2.57 ± 0.06 % [36]. The effective b branching fractions used in the different MC generators were corrected to those listed in Table 2 in order to account for their influence on the overall acceptance, and on the shape of the predicted beauty contributions.

The measured beauty fraction in the inclusive sample, corrected for detector acceptance and branching fractions, was used to obtain the cross section for the process $ep \to eb\bar{b}X \to eD^{*\pm}\mu X$ in the visible kinematic range $p_T^{D^*} > 1.9$ GeV, $-1.5 < \eta^{D^*} < 1.5$, $p_T^\mu > 1.4$ GeV and $-1.75 < \eta^\mu < 1.3$ as:

$$\sigma_{\mathrm{vis}}(ep \to eb\bar{b}X \to eD^{*\pm}\mu X) = 160 \pm 37(\mathrm{stat.})^{+30}_{-57}(\mathrm{syst.})\ \mathrm{pb}. \quad (5)$$

This includes both unlike- and like-sign $D^*\mu$ combinations. The leading-order cross sections predicted by PYTHIA and HERWIG in the same kinematic range are $\sigma_{\mathrm{vis}}(ep \to eb\bar{b}X \to eD^*\mu X) = 80$ and 38 pb, respectively. The measured cross section is larger than, but compatible with, the FMNR$\otimes$PYTHIA NLO prediction

$$\sigma_{\mathrm{vis}}^{\mathrm{NLO}}(ep \to eb\bar{b}X \to eD^{*\pm}\mu X) = 67^{+20}_{-11}(\mathrm{NLO})^{+13}_{-9}(\mathrm{frag.} \oplus \mathrm{br.})\ \mathrm{pb}, \quad (6)$$

where the first error refers to the uncertainties of the FMNR parton level calculation, and the second error refers to the uncertainties related to fragmentation and decay.

For the photoproduction subsample, a visible cross section in the kinematic range $Q^2 < 1$ GeV^2 and $0.05 < y < 0.85$ was obtained:

$$\sigma_{\mathrm{vis},\gamma p}(ep \to eb\bar{b}X \to eD^{*\pm}\mu X) = 115 \pm 29(\mathrm{stat.})^{+21}_{-27}(\mathrm{syst.})\ \mathrm{pb}. \tag{7}$$

This can be compared to the NLO prediction from FMNR$\otimes$PYTHIA,

$$\sigma^{\mathrm{NLO}}_{\mathrm{vis},\gamma p}(ep \to eb\bar{b}X \to eD^{*\pm}\mu X) = 54^{+15}_{-10}(\mathrm{NLO})^{+10}_{-7}(\mathrm{frag.} \oplus \mathrm{br.})\ \mathrm{pb}. \tag{8}$$

As in the inclusive case, the NLO prediction underestimates the measured cross section by about a factor of 2, but is compatible with the measurement (Table 3).

From the DIS sample, a visible cross section in the kinematic range $Q^2 > 2$ GeV^2, $0.05 < y < 0.7$ and $p_T^{D^*} > 1.5$ GeV (other D^* and muon cuts as for Eq.(5)) was obtained

$$\sigma_{\mathrm{vis,DIS}}(ep \to eb\bar{b}X \to eD^{*}\mu X) = 58 \pm 29(\mathrm{stat.})^{+11}_{-20}(\mathrm{syst.})\ \mathrm{pb}. \tag{9}$$

Again, the cross sections obtained from RAPGAP (used to compute acceptance corrections for the central signal extraction) and HERWIG (used for systematic checks, particularly with regard to differences in the $b\bar{b}$ correlations) in the same kinematic regime are considerably lower, $\sigma(ep \to eb\bar{b}X \to eD^*\mu X) = 26$ and 10 pb, respectively. An NLO prediction is not available for this kinematic region.

8.2 Comparison to H1 results

A photoproduction cross section similar to Eq.(7) in a slightly different kinematic range, $p_T^{D^*} > 1.5$ GeV, $|\eta^{D^*}| < 1.5$, $p^\mu > 2.0$ GeV, $|\eta^\mu| < 1.735$, $Q^2 < 1$ GeV^2 and $0.05 < y < 0.75$ has been obtained by the H1 collaboration [12]

$$\sigma^{\mathrm{H1}}_{\mathrm{vis},\gamma p}(ep \to eb\bar{b}X \to eD^{*\pm}\mu X; \mathrm{H1}) = 206 \pm 53(\mathrm{stat.}) \pm 35(\mathrm{syst.})\ \mathrm{pb}. \tag{10}$$

The ZEUS cross section of Eq.(7) extrapolated to the H1 kinematic range using FMNR$\otimes$PYTHIA is

$$\sigma_{\mathrm{vis},\gamma p}(ep \to eb\bar{b}X \to eD^{*\pm}\mu X; \mathrm{H1}) = 135 \pm 33(\mathrm{stat.})^{+24}_{-31}(\mathrm{syst.})\ \mathrm{pb}, \tag{11}$$

which is somewhat smaller, but in agreement within errors.

The corresponding FMNR$\otimes$PYTHIA NLO prediction is

$$\sigma^{\mathrm{NLO}}_{\mathrm{vis},\gamma p}(ep \to eb\bar{b}X \to eD^{*\pm}\mu X; \mathrm{H1}) = 61^{+17}_{-12}(\mathrm{NLO})^{+12}_{-8}(\mathrm{frag.} \oplus \mathrm{br.})\ \mathrm{pb}. \tag{12}$$

This is larger than the NLO cross section evaluated by H1 [12] due to the inclusion of the hadron-like photon contribution, the inclusion of secondary-muon branching fractions for D^* and μ from the same b quark (Table 2), and a detailed simulation of the kinematics of the $b \to B \to D^*$ chain rather than direct collinear fragmentation of b quarks into D^* mesons. The data to NLO ratio is consistent with the results in the ZEUS kinematic range.

8.3 Cross sections for $D^*\mu$ from the same b quark

In all the cross sections evaluated above, a significant part of the systematic error arises from the fraction of the beauty contribution in the charm enriched or like-sign regions, where it cannot be well measured ($\Delta R > 2$ region in Fig. 4a; Figs. 4b and 4d). This fraction depends on details of the description of $b\bar{b}$ correlations in the MC used for the signal extraction. In the beauty-enriched low-ΔR unlike-sign region, which dominates the fit of the beauty fraction, about 95% of the $D^*\mu$ pairs are produced from the same parent b quark. The systematic error can thus be reduced by reinterpreting the measurements in terms of cross sections for this subprocess only. The corresponding cross section for photoproduction of a D^* and μ from the same b quark (always unlike sign, same kinematic cuts as for Eq.(7)) is

$$\sigma_{\mathrm{vis},\gamma p}(ep \to eb(\bar{b})X, b(\bar{b}) \to eD^*\mu X) = 52 \pm 13(\mathrm{stat.})^{+9}_{-11}(\mathrm{syst.})\ \mathrm{pb} \tag{13}$$

where $b(\bar{b})$ stands for the sum of b and $\bar{b}$ cross sections, and all other cuts remain the same.

This is comparable with the NLO prediction

$$\sigma^{\mathrm{NLO}}_{\mathrm{vis},\gamma p}(ep \to eb(\bar{b})X, b(\bar{b}) \to eD^*\mu X) = 29^{+8}_{-5}(\mathrm{NLO})^{+5}_{-4}(\mathrm{frag.} \oplus \mathrm{br.})\ \mathrm{pb}. \tag{14}$$

For the DIS kinematic range (same as Eq.(9))

$$\sigma_{\mathrm{vis,DIS}}(ep \to eb(\bar{b})X, b(\bar{b}) \to eD^*\mu X) = 28 \pm 14(\mathrm{stat.})^{+5}_{-10}(\mathrm{syst.})\ \mathrm{pb} \tag{15}$$

is obtained.

8.4 Parton-level cross sections

For a direct comparison with the NLO parton level predictions, the measured visible cross sections are extrapolated to cross sections at b quark level. In order to minimize the systematic error the b-level cross section is quoted for individual b (or $\bar{b}$) production rather than for correlated $b\bar{b}$-pair production, i.e. using the cross sections displayed in Eqns. 13) and (15).

A significant fraction of the parent b quarks of the selected events is expected to have very low p_T^b values [22]. Therefore, cross sections with no cut on p_T^b have been measured. Furthermore, there is a strong correlation between the pseudorapidity of the $D^*\mu$ system and the longitudinal rapidity of the parent b quark[4]. In order to reflect the limited angular acceptance of the detector for both the D^* and the muon, the cross-section measurement was restricted to $\zeta^b < 1$. In this range, restricted to photoproduction, the p_T^b and ζ^b distributions of PYTHIA (after parton showering) agree with the central NLO b-quark spectra from FMNR to within ±15% [22]. Therefore, PYTHIA was used to extrapolate the visible cross section for the photoproduction region. Similarly, the corresponding RAPGAP spectra for the DIS case agree [22] with the central NLO predictions from HVQDIS.

The extrapolation implies additional systematic uncertainties from the b-quark fragmentation (+5/-15%) and decay (±9%) and the details of the shape of the p_T^b spectrum (±5%). The extrapolation was calculated assuming the validity of the NLO p_T^b shape and therefore is valid only in this theoretical framework; the uncertainty for the visible cross section corresponding to a potential deviation from this shape, namely the reweighting of the $p_T^{D^*\mu}$ spectrum, is removed. The result for the extrapolated cross section for $\zeta^b < 1,\ Q^2 < 1\ \text{GeV}^2,\ 0.05 < y < 0.85$ and $m_b = 4.75$ GeV is:

$$\sigma_{\gamma p}(ep \to b(\bar{b})X) = 11.9 \pm 2.9(\text{stat.})^{+1.8}_{-3.3}(\text{syst.})\ \text{nb}. \tag{16}$$

The corresponding result for the extrapolated cross section for $\zeta^b < 1,\ Q^2 > 2\ \text{GeV}^2,\ 0.05 < y < 0.7$ and $m_b = 4.75$ GeV is:

$$\sigma_{DIS}(ep \to b(\bar{b})X) = 3.6 \pm 1.8(\text{stat.})^{+0.5}_{-1.4}(\text{syst.})\ \text{nb}. \tag{17}$$

These cross sections are to be compared to the NLO prediction for the same kinematic range using the FMNR calculation of

$$\sigma_{\gamma p}^{NLO}(ep \to b(\bar{b})X) = 5.8^{+2.1}_{-1.3}\ \text{nb}, \tag{18}$$

and to the NLO HVQDIS prediction of

$$\sigma_{DIS}^{NLO}(ep \to b(\bar{b})X) = 0.87^{+0.28}_{-0.16}\ \text{nb}. \tag{19}$$

These cross sections are presented in Fig. 6. The ratio of measured to predicted cross sections in the photoproduction region remains the same as the ones obtained from the comparison at visible level (Table 3). This confirms the self-consistency of the used extrapolation procedure.

[4] $\zeta^b \equiv \frac{1}{2}\ln\frac{(E+p_z)^b}{(E-p_z)^b}$

8.5 Comparison to previous ZEUS measurements

In order to compare the photoproduction cross section to previous ZEUS results [10, 11], the cross sections Eq.(13) or equivalently Eq.16), already referring to the production of a single b quark, need to be translated into a differential cross section, $\frac{d\sigma}{dp_T^b}$, in the pseudorapidity range $|\eta^b| < 2$ [10]. The median p_T^b value for events satisfying the cuts for (13) is 6.5 GeV [22]. The measured cross section Eq.(13) is therefore extrapolated to this value using FMNR⊗PYTHIA, yielding

$$\frac{d\sigma}{dp_T^b}(p_T^b = 6.5\text{ GeV}, |\eta^b| < 2) = 0.30 \pm 0.07(\text{stat.})^{+0.05}_{-0.06}(\text{syst.})\text{ nb.} \tag{20}$$

This result is compared to theory and previous measurements in Fig. 7. It is higher than, but consistent with, these measurements.

9 Conclusions

Cross sections for beauty production in *ep* collisions at HERA have been measured in both the photoproduction and DIS regimes using an analysis technique based on the detection of a muon and D^*. Agreement is obtained with the corresponding H1 result. Since the analysis is sensitive to b-quark production near the kinematic threshold, the measured visible cross sections were extrapolated to b-quark cross sections without an explicit cut on p_T^b. Both at visible and at quark level, the measured cross sections exceed the NLO QCD predictions, but are compatible within the errors. The data to NLO ratio is also larger than, but compatible with, previous ZEUS measurements of the b production cross section at higher p_T^b.

Acknowledgements

We thank the DESY Directorate for their strong support and encouragement. The remarkable achievements of the HERA machine group were essential for the successful completion of this work and are greatly appreciated. We are grateful for the support of the DESY computing and network services. The design, construction and installation of the ZEUS detector have been made possible owing to the ingenuity and effort of many people who are not listed as authors. It is also a pleasure to thank S. Frixione for help with the theoretical predictions.

References

[1] S. Frixione et al., Nucl. Phys. **B 412**, 225 (1994);
S. Frixione, P. Nason and G. Ridolfi, Nucl. Phys. **B 454** (1995);
M. Cacciari, S. Frixione and P. Nason, JHEP **0103**, 006 (2001).

[2] B.W. Harris and J. Smith, Nucl. Phys. **B 452**, 109 (1995);
B. W. Harris and J. Smith, Phys. Lett. **B 353**, 535 (1995). Erratum-ibid **B 359** (1995) 423;
B.W. Harris and J. Smith, Phys. Rev. **D 57**, 2806 (1998).

[3] UA1 Coll.., C. Albajar et al., Phys. Lett. **B 186**, 237 (1987);
UA1 Coll., C. Albajar et al., Phys. Lett. **B 256**, 121 (1991). Erratum in Phys. Lett. B 262, 497 (1991);
UA1 Coll., C. Albajar et al., Z. Phys. **C 61**, 41 (1994).

[4] CDF Coll., F. Abe et al., Phys. Rev. Lett. **71**, 500 (1993);
CDF Coll., F. Abe et al., Phys. Rev. Lett. **71**, 2396 (1993);
CDF Coll., F. Abe et al., Phys. Rev. Lett. **75**, 1451 (1995);
CDF Coll., F. Abe et al., Phys. Rev. **D 53**, 1051 (1996);
CDF Coll., D. Acosta et al., Phys. Rev. **D 65**, 052005 (2002);
CDF Coll., D. Acosta et al., Phys. Rev. **D 71**, 032001 (2005);
DØ Coll., S. Abachi et al., Phys. Rev. Lett. **74**, 3548 (1995);
DØ Coll., B. Abbott et al., Phys. Lett. **B 487**, 264 (2000);
DØ Coll., B. Abbott et al., Phys. Rev. Lett. **84**, 5478 (2000);
DØ Coll., B. Abbott et al., Phys. Lett. **85**, 5068 (2000).

[5] L3 Coll., M. Acciarri et al., Phys. Lett. **B 503**, 10 (2000);
L3 Coll., P. Achard et al., Phys. Lett. **B 619**, 71 (2005).

[6] WA78 Coll., M. Catanesi et al., Phys. Lett. **B 202**, 453 (1988);
E672/E706 Coll., R. Jesik et al., Phys. Rev. Lett. **74**, 495 (1995).

[7] E771 Coll., T. Alexopoulos et al., Phys. Rev. Lett. **82**, 41 (1999);
D.M. Jansen et al., Phys. Rev. Lett. **74**, 3118 (1995);
HERA–B Coll., I. Abt et al., Eur. Phys. J. **C 26**, 345 (2003).

[8] H1 Coll., C. Adloff et al., Phys. Lett. **B 467**, 156 (1999);
ZEUS Coll., J. Breitweg et al., Eur. Phys. J. **C 18**, 625 (2001).

[9] H1 Coll., A. Aktas et al., Eur. Phys. J. **C 41**, 453 (2005);
H1 Coll., A. Aktas et al., Eur. Phys. J. **C 40**, 349 (2005);
H1 Coll., A. Aktas et al., Eur. Phys. J. **C 45**, 23 (2006);
H1 Coll., A. Aktas et al., Preprint hep-ex/0605016, 2006.

[10] ZEUS Coll., S. Chekanov et al., Phys. Rev. **D 70**, 12008 (2004).

[11] ZEUS Coll., S. Chekanov et al., Phys. Lett. **B 599**, 173 (2004).

[12] H1 Coll., A. Aktas et al., Phys. Lett. **B 621**, 56 (2005).

[13] ZEUS Coll., U. Holm (ed.), *The ZEUS Detector*. Status Report (unpublished), DESY (1993), available on `http://www-zeus.desy.de/bluebook/bluebook.html`.

[14] N. Harnew et al., Nucl. Inst. Meth. **A 279**, 290 (1989);
B. Foster et al., Nucl. Phys. Proc. Suppl. **B 32**, 181 (1993);
B. Foster et al., Nucl. Inst. Meth. **A 338**, 254 (1994).

[15] M. Derrick et al., Nucl. Inst. Meth. **A 309**, 77 (1991);
A. Andresen et al., Nucl. Inst. Meth. **A 309**, 101 (1991);
A. Caldwell et al., Nucl. Inst. Meth. **A 321**, 356 (1992);
A. Bernstein et al., Nucl. Inst. Meth. **A 336**, 23 (1993).

[16] A. Bamberger et al., Nucl. Inst. Meth. **A 401**, 63 (1997).

[17] ZEUS Coll., S. Chekanov et al., Eur. Phys. J. **C 21**, 443 (2001).

[18] G. Abbiendi et al., Nucl. Inst. Meth. **A 333**, 342 (1993).

[19] J. Andruszków et al., Preprint DESY-92-066, DESY, 1992;
ZEUS Coll., M. Derrick et al., Z. Phys. **C 63**, 391 (1994);
J. Andruszków et al., Acta Phys. Pol. **B 32**, 2025 (2001).

[20] ZEUS Coll., S. Chekanov et al., Nucl. Phys. **B 729**, 492 (2005).

[21] F. Jacquet and A. Blondel, *Proceedings of the Study for an ep Facility for Europe*, U. Amaldi (ed.), p. 391. Hamburg, Germany (1979). Also in preprint DESY 79/48.

[22] A. Longhin, *Measurement of beauty production at HERA with a* $D^* + \mu$ *tag*. Ph.D. Thesis, Università di Padova, Padova (Italy), Report DESY-THESIS-2004-050, Università di Padova and INFN, 2004.

[23] T. Sjöstrand, Comp. Phys. Comm. **82**, 74 (1994).

[24] H. Jung, Comp. Phys. Comm. **86**, 147 (1995).

[25] G. Marchesini et al., Comp. Phys. Comm. **67**, 465 (1992).

[26] R. Brun et al., GEANT3, Technical Report CERN-DD/EE/84-1, CERN, 1987.

[27] J. Binnewies, B.A. Kniehl and G. Kramer, Z. Phys. **C 76**, 677 (1997);
B.A. Kniehl, G. Kramer and M. Spira, Z. Phys. **C 76**, 689 (1997);
J. Binnewies, B.A. Kniehl and G. Kramer, Phys. Rev. **D 58**, 014014 (1998).

[28] A. Lipatov and N. Zotov, Preprint hep-ph/0601240, 2006;
A. Lipatov and N. Zotov, Preprint hep-ph/0603017, 2006.

[29] CTEQ Coll., H.L. Lai et al., Eur. Phys. J. **C 12**, 375 (2000).

[30] M. Glück, E. Reya, and A. Vogt, Phys. Rev. **D 46**, 1973 (1992).

[31] Adriana Elizabeth Nuncio-Quiroz, ZEUS Coll., talk at XIV International Workshop on Deep Inelastic Scattering, Tsukuba, Japan, 20-24 April 2006; to appear in proceedings.

[32] T. Sjöstrand, L. Lönnblad, and S. Mrenna, Preprint hep-ph/0108264, 2001.

[33] S. Frixione and B.R. Webber, JHEP **06**, 029 (2002);
S. Frixione, P. Nason and R.B. Webber, JHEP **08**, 007 (2003).

[34] C. Peterson et al., Phys. Rev. **D 27**, 105 (1983).

[35] B. Andersson, G. Gustafson and B. Söderberg, Z. Phys. **C 20**, 317 (1983);
B.R. Webber, Nucl. Phys. **B 238**, 492 (1984);
T. Sjöstrand, Comp. Phys. Comm. **39**, 347 (1986).

[36] Particle Data Group, S. Eidelman et al., Phys. Lett. **B 592**, 1 (2004).

[37] C.F. von Weizsäcker, Z. Phys. **88**, 612 (1934). In German;
E.J. Williams, Phys. Rev. **45**, 729 (1934);
S. Frixione et al., Phys. Lett. **B 319**, 339 (1993).

[38] ZEUS Coll., S. Chekanov et al., Phys. Rev. **D 69**, 012004 (2004).

[39] ZEUS Coll., S. Chekanov et al., Phys. Lett. **B 590**, 143 (2004).

Sample	Cuts	Data	Beauty	Charm prompt μ	Charm fake μ	Fake D^*
		Inclusive sample				
unlike sign	$\Delta R < 2$, $3 < M < 5$ GeV	41	28.8	3.6	2.5	11.2
	$\Delta R > 2$	93	6.5	56.5	18.4	6.4
like sign	$\Delta R < 2$, $3 < M < 5$ GeV	18	1.6	0.7	1.3	9.2
	$\Delta R > 2$	36	11.1	2.0	21.2	5.2
		γp				
unlike sign	$\Delta R < 2$, $3 < M < 5$ GeV	31	23.6	1.2	1.6	8.3
	$\Delta R > 2$	79	6.2	48.8	14.0	6.2
like sign	$\Delta R < 2$, $3 < M < 5$ GeV	14	1.5	0.6	0.4	6.9
	$\Delta R > 2$	28	9.1	1.9	17.1	5.2
		DIS				
unlike sign	$\Delta R < 2$, $3 < M < 5$ GeV	11	8.1	1.6	0.5	1.0
	$\Delta R > 2$	14	3.2	6.1	1.2	3.9
like sign	$\Delta R < 2$, $3 < M < 5$ GeV	3	1.2	0.1	0.5	0.3
	$\Delta R > 2$	10	5.0	0.2	2.6	1.2

Table 1: *Composition of the final $D^*\mu$ event samples (number of events).*

channel	branching fraction w/o B^0-$\bar{B}^0$ mixing
$b \to D^{*\pm}$ inclusive	17.3 ± 2.0 % 86 ± 3 % D^{*+}, 14 ± 3 % D^{*-}
$b \to \mu^-$ direct	10.95 ± 0.27 %
$b \to \mu^+$ indirect	8.27 ± 0.40 %
$b \to \mu^-$ indirect	2.21 ± 0.50 %
all $b \to \mu^\pm$	21.43 ± 0.70 %
$b\bar{b} \to D^{*\pm}\mu^\pm$ (diff. b's)	4.34 ± 0.92 %
$b\bar{b} \to D^{*\pm}\mu^\mp$ (diff. b's)	3.08 ± 0.60 %
$b \to D^{*+}\mu^-$ direct	2.75 ± 0.19 %
$b \to D^{*\pm}\mu^\mp$ indirect	1.09 ± 0.27 %
all $b \to D^{*\pm}\mu^\mp$	3.84 ± 0.33 %

Table 2: *Branching fractions assumed for cross-section determinations. The indirect contributions include cascade decays into muons via charm, anticharm, $\tau^\pm$ and J/ψ. The values in the Table are given before the inclusion of the effect of B^0-$\bar{B}^0$ mixing (mixing parameter $\chi = 0.1257 \pm 0.0042$).*

cross section	measured	NLO QCD	ratio
inclusive, visible Eq.(5)	$160 \pm 37^{+30}_{-57}$ pb	67^{+24}_{-14} pb	$2.4^{+0.9}_{-1.3}$
γp, visible Eq.(7)	$115 \pm 29^{+21}_{-27}$ pb	54^{+18}_{-12} pb	$2.1^{+0.8}_{-1.0}$
DIS, visible Eq.(9)	$58 \pm 29^{+11}_{-20}$ pb	-	-
γp, vis. same b Eq.(13)	$52 \pm 13^{+9}_{-11}$ pb	29^{+9}_{-6} pb	$1.8^{+0.7}_{-0.8}$
DIS, vis. same b Eq.(15)	$28 \pm 14^{+5}_{-10}$ pb	-	-
γp, b quark Eq.(16)	$11.9 \pm 2.9^{+1.8}_{-3.3}$ nb	$5.8^{+2.1}_{-1.3}$ nb	$2.0^{+0.8}_{-1.1}$
DIS, b quark Eq.(17)	$3.6 \pm 1.8^{+0.5}_{-1.4}$ nb	$0.87^{+0.28}_{-0.16}$ nb	$4.2^{+2.3}_{-2.9}$
γp, b differential Eq.(20)	$0.30 \pm 0.07^{+0.05}_{-0.06}$ nb/GeV	$0.16^{+0.04}_{-0.02}$ nb/GeV	$1.8^{+0.7}_{-0.8}$

Table 3: *Comparison of measured and predicted cross sections. For the measured cross sections, the first error is statistical, and the second systematic. For the QCD prediction, the first error is related to the parton-level NLO calculation, while the second (where present) reflects the uncertainties of fragmentation and decay to the visible final state. The number in parentheses refers to the corresponding label for each cross section, see text. For the definition of the kinematic range of each cross section see text.*

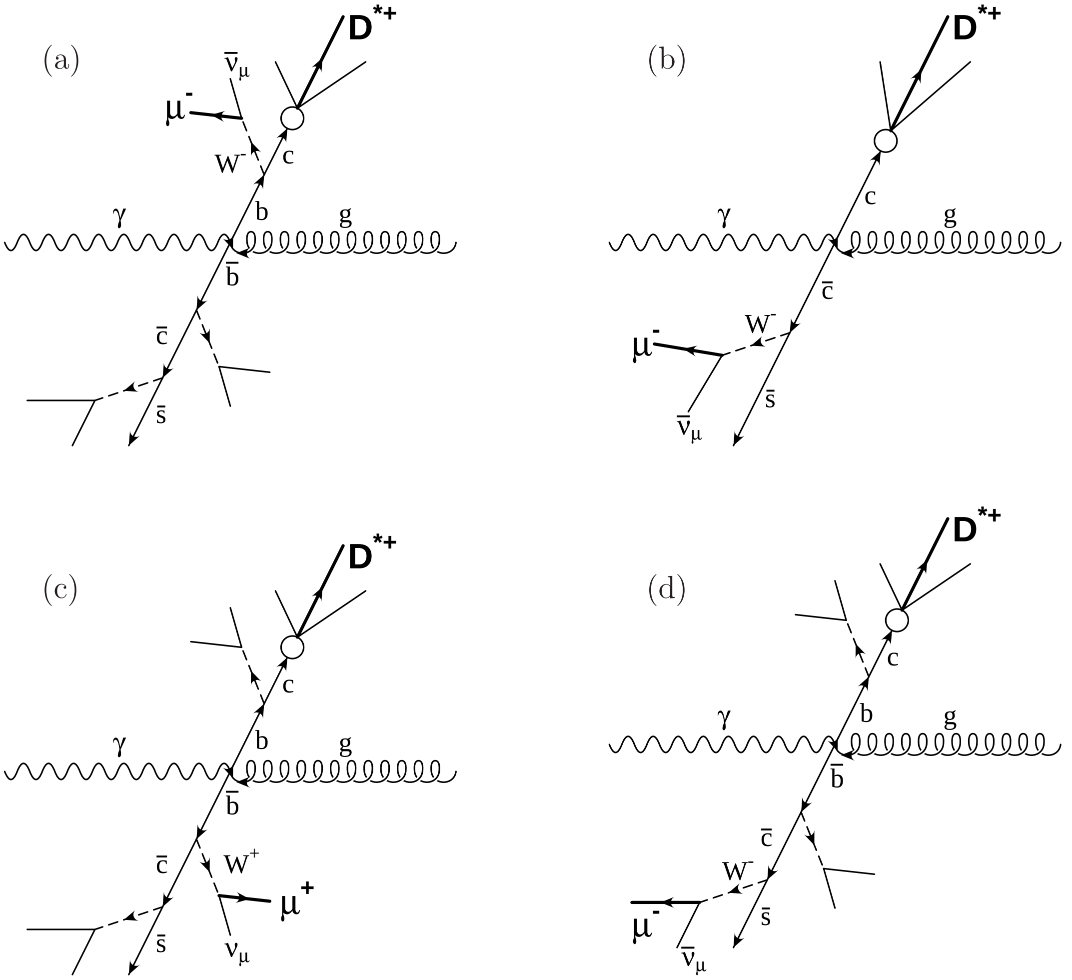

Figure 1: *Processes leading to $D^*\mu$ final states.*

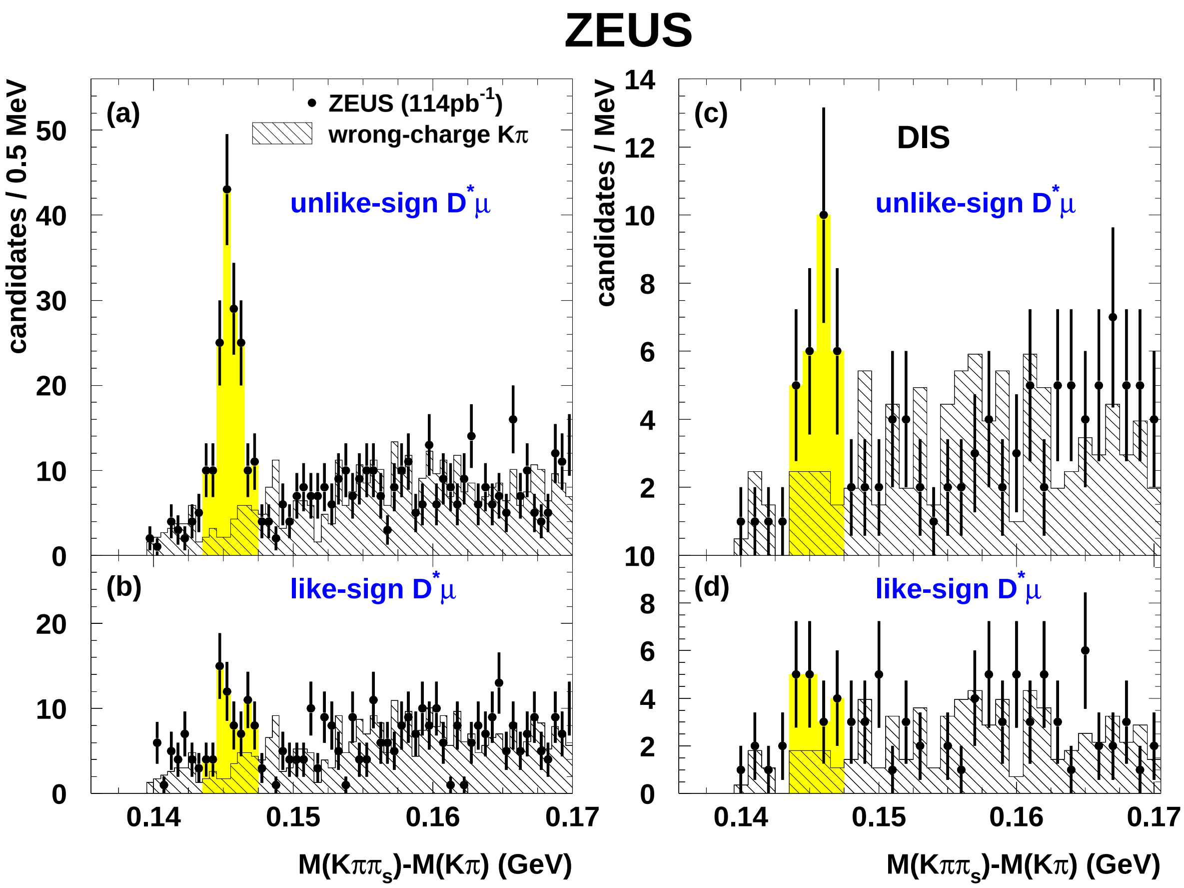

Figure 2: *Distribution of ΔM for data (full circles) and combinatorial background (hatched histogram) for (a) inclusive unlike-sign (b) inclusive like-sign (c) DIS unlike-sign and (d) DIS like-sign muon-D^* combinations. The D^* signal region is indicated by the shaded area.*

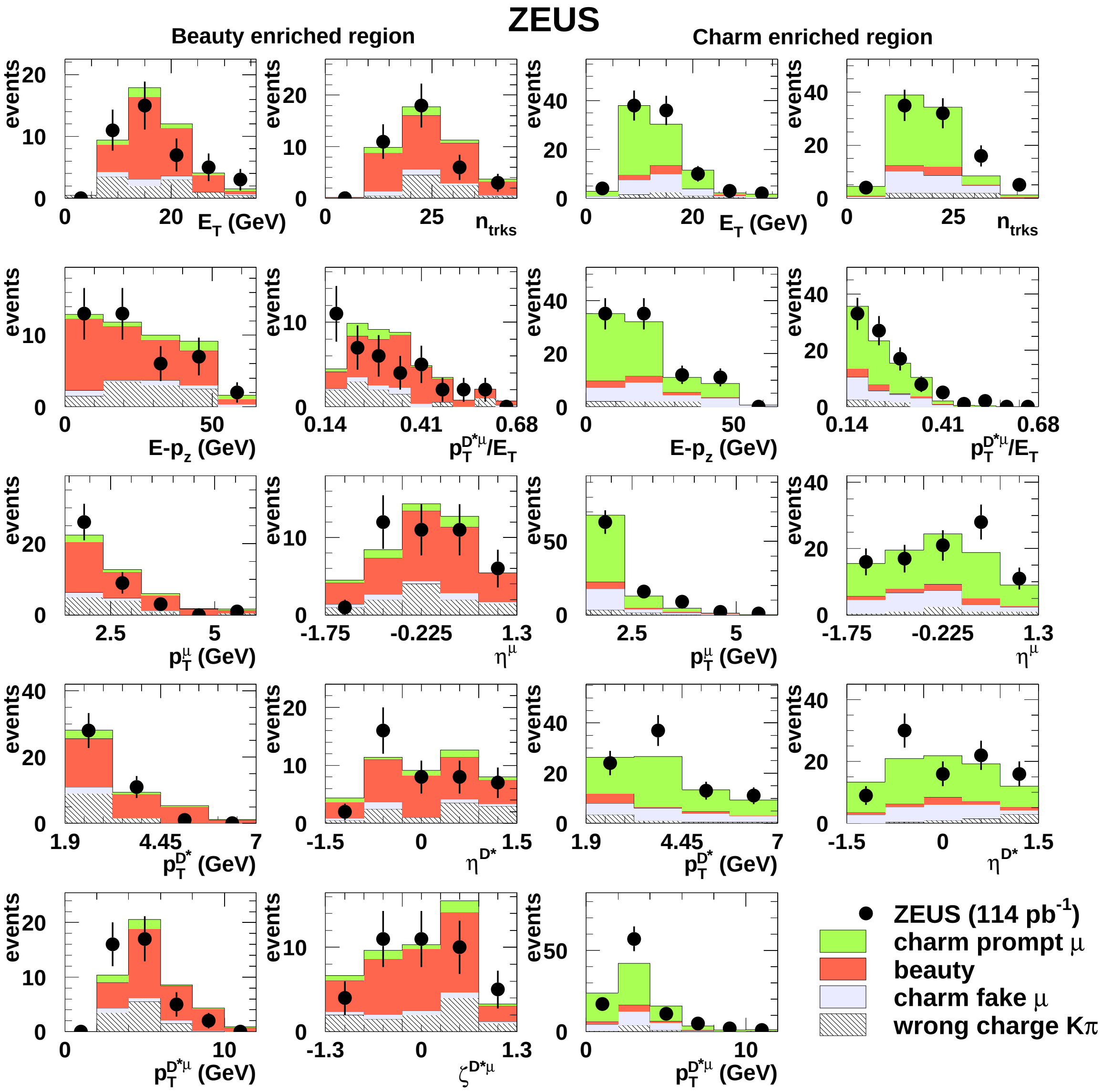

Figure 3: *Distributions of variables used in the event selection or relevant for the event kinematics, for the unlike-sign inclusive sample after all cuts. All variables are defined in the text except n_{trks} (total number of tracks) and $\zeta^{D^*\mu}$ (rapidity of the $D^*\mu$ system). The distributions are shown separately for the beauty- and charm-enriched regions as defined in Section 5. The beauty, charm, fake-muon and wrong-charge $K\pi$ background distributions are indicated by different hatch styles, and normalized to the fractions determined later in the analysis.*

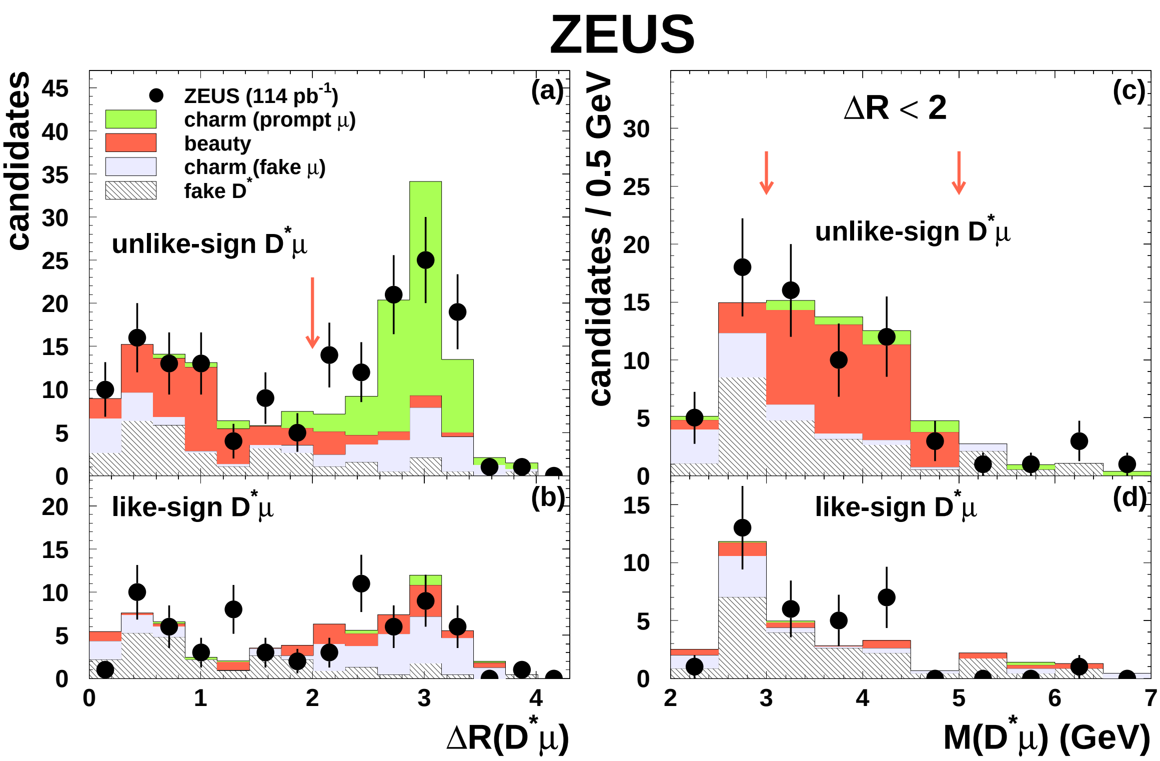

Figure 4: *(a),(b) Distribution of $\Delta R(D^*\mu)$ and (c),(d) $M(D^*\mu)$ for inclusive data (full circles), beauty and charm signal, fake-μ and fake-D^* backgrounds. The latter are distinguished by different hatch styles. Unlike-sign and like-sign $D^*\mu$ combinations are shown separately. Cuts described in the text are indicated by the arrows.*

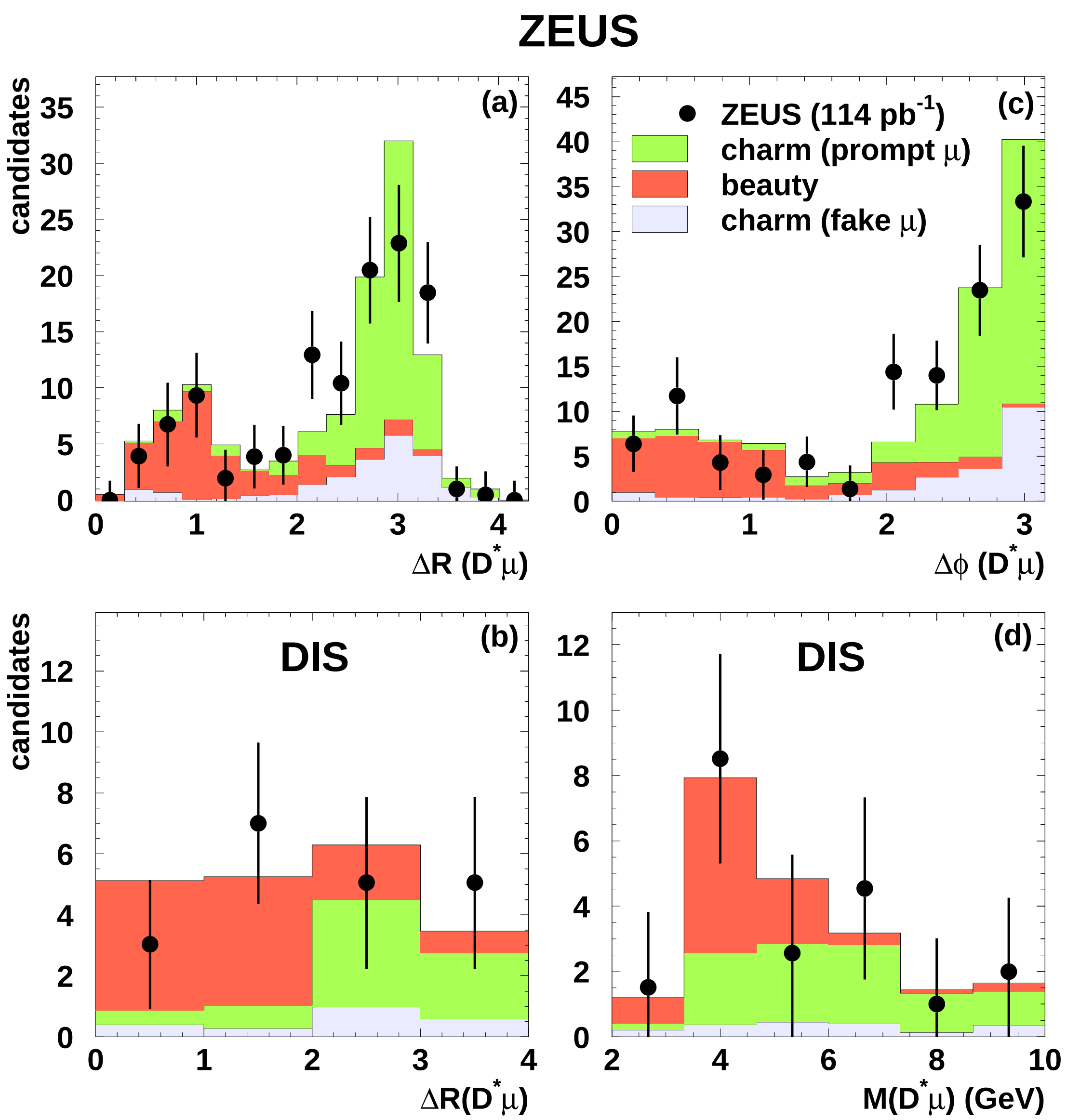

Figure 5: *Distributions of $\Delta R(D^*\mu)$ (a), $\Delta\phi(D^*\mu)$ (c) for unlike-sign events in the inclusive sample, $\Delta R(D^*\mu)$ (b) and $M(D^*\mu)$ (d) for for unlike-sign events in the DIS sample after subtraction of the fake-D^* background. Data points (full circles) are shown together with the fitted contributions from beauty and charm, as indicated in the legend. The fake-muon contribution from charm is shown separately, but fitted together with the charm contribution.*

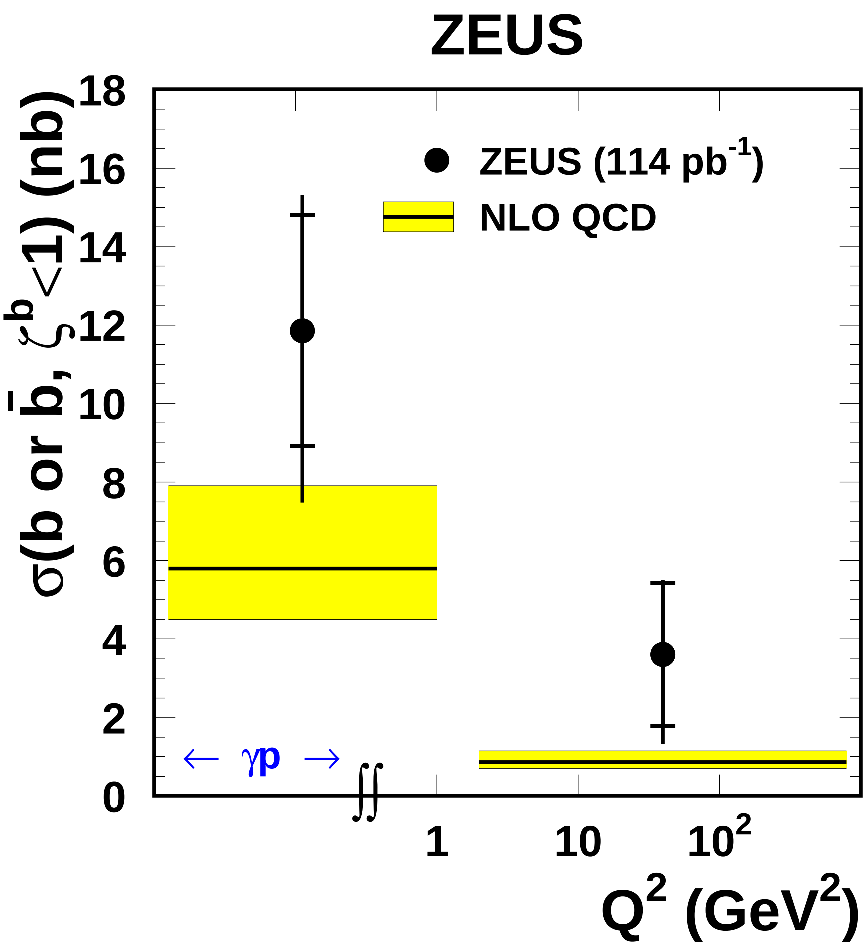

Figure 6: *Cross section for single b or $\bar{b}$-quark production in the rapidity range $\zeta^b < 1$ for photoproduction (left) and DIS (right), compared to NLO QCD predictions from FMNR (left) and HVQDIS (right). The γp cross section is for $0.05 < y < 0.85$, and the DIS cross section for $0.05 < y < 0.7$. The cross sections are integrated over the indicated Q^2 ranges, and over the full p_T^b range.*

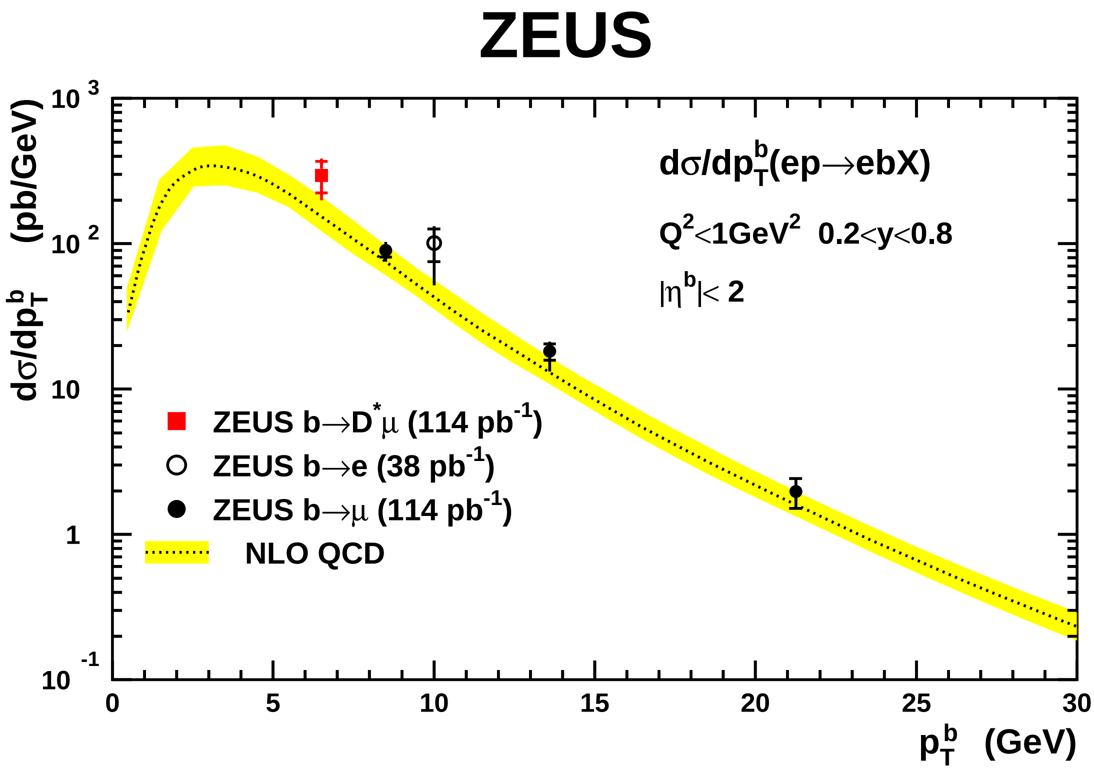

Figure 7: *Differential cross-section* $\frac{d\sigma}{dp_T^b}$ *of this analysis (filled square) compared to measurements from previous ZEUS analyses, after rescaling to the kinematic range indicated in the Figure.*